The effect of spiral arms on star formation in the Galaxy

T. J. T. Moore,[1]⋆ J. S. Urquhart,[2,3] L. K. Morgan[1] and M. A. Thompson[4]

[1]*Astrophysics Research Institute, Liverpool John Moores University, Twelve Quays House, Egerton Wharf, Birkenhead CH41 1LD*
[2]*Australia Telescope National Facility, CSIRO Astronomy and Space Science, PO Box 76, Epping, NSW 1710, Australia*
[3]*Max-Planck-Institut für Radioastronomie, Auf dem Hügel 69, 53121 Bonn, Germany*
[4]*Centre for Astrophysics Research, Science & Technology Research Institute, University of Hertfordshire, College Lane, Hatfield, Herts AL10 9AB*

ABSTRACT

We have examined the ratio between the integrated luminosity of massive young stellar objects detected by the Red MSX Source (RMS) survey and the mass of molecular clouds in the Galactic Ring Survey (GRS) region, as a function of Galactocentric radius. The results indicate that 60–80 per cent of the observed increases in the star formation rate density associated with spiral-arm features are due to source crowding within the arms. Of the remainder, most of the increase in the inner Sagittarius arm is due to an enhancement in the simple star formation efficiency, i.e. in the number of RMS sources per unit molecular gas mass. In the inner Perseus arm, the residual increase is due to a higher than average mean source luminosity, which implies a top-heavy initial mass function, and this is entirely due to the presence, in the GRS region, of the W49 star-forming complex, which appears to be exceptional in its nature. The results also suggest that there is little or no increase in the star formation efficiency on kiloparsec scales in the Scutum tangent region which includes W43. We discuss the possible role played by the spiral arms in influencing the star formation efficiency and conclude that the most likely mechanisms are related to orbit crowding within the arms.

Key words: stars: formation – ISM: clouds – Galaxy: structure.

1 INTRODUCTION

The role that spiral arms play in affecting the process and efficiency of star formation in galaxies is not yet clear. They may simply organize the gas of the interstellar medium (ISM), along with its molecular clouds, into regions of higher density, thus increasing the local star formation rate (SFR) density. Increases in star formation efficiency (SFE) could result from such crowding, via a rise in the incidence or strength of local feedback, e.g. from earlier massive star formation, inducing additional star formation. On the other hand, spiral arms may be more direct triggers of star formation. They may raise the probability of cloud–cloud collisions or increase the efficiency with which molecular clouds form from the neutral gas, via the shocks expected as the ISM gas enters the arm, or by altering the internal state, i.e. the average mass, velocity dispersion or lifetime of molecular clouds so as to affect their internal SFE.

Heyer & Terebey (1998) found evidence, in H I and CO data in W3/4/5, that the molecular fraction of the gas content in the outer Perseus spiral arm was around 10 times higher than in the inter-arm regions on the line of sight. This result implies that spiral arms dramatically raise the efficiency with which molecular clouds are produced out of the neutral gas. In turn, this suggests that spiral

density waves trigger additional star formation, via the creation of new molecular clouds, as modelled by e.g. Dobbs, Bonnell & Pringle (2006). In contrast, recent observations of two external spiral galaxies by Foyle et al. (2010) indicate that the $H_2/H I$ fraction and the infrared (IR)- and ultraviolet (UV)-traced SFE are not significantly enhanced in spiral arms relative to the inter-arm gas. Also, Leroy et al. (2008) conclude that the fraction of giant molecular clouds (GMCs) formed from H I is governed by ISM physics acting on relatively small scales, i.e. the H_2 formation/destruction rate balance and stellar feedback. Krumholz, McKee & Tumlinson (2009) predict that, except in starburst conditions, molecular-cloud properties are dominated by internal radiative feedback and not the environment.

Dobbs, Burkert & Pringle (2011) suggest that spiral arms are mainly organizing features, whose main effect on the ISM is to delay and crowd the gas, which is deflected from circular orbits while within the arm. The SFR is increased indirectly by enabling longer lived and more massive GMCs. Roman-Duval et al. (2010) conclude from observations that molecular clouds within spiral arms are more long lived than in the inter-arm gas, which would lengthen the star formation time-scale for a typical cloud, increasing the SFE as a result. If larger or denser clouds are formed, it may be significant. Krumholz et al. (2010) predict that the column density of clouds affects the mass function of clusters that form within them via radiative heating which suppresses fragmentation in the

⋆E-mail: tjtm@astro.livjm.ac.uk

higher column clouds but does not significantly affect the overall SFR/E.

It is also likely that spiral arms are different from each other (e.g. Benjamin et al. 2005). Also, the inner and outer portions of spiral arms may influence star formation differently. The entry shock experienced by the ISM gas entering a spiral arm should only exist inside the corotation radius, where there is a differential velocity between the spiral pattern speed and the orbital rotation speed of the galactic ISM. Outside this radius (thought to be just beyond the solar circle in the Milky Way; Lépine et al. 2011), supernovae may be the dominant mechanism determining the state of the ISM and, hence, star formation (e.g. Kobayashi et al. 2008; Dib et al. 2009). The presence of the Galactic bar may also affect star formation, especially near the bar ends where the pattern rotates at the same speed as the adjacent orbiting gas and where crowding between orbits in the bar potential and external circular orbits may create a higher cloud collision rate.

Despite the abundance of clues, or perhaps because of it, our knowledge of the effect of spiral arms on the SFR or efficiency is still poorly developed and the main questions about the relationship between large-scale Galactic structure and star formation remain unanswered.

This paper reports the results of an investigation into the dependence of the efficiency of star formation on Galactocentric radius and proximity to Galactic spiral arms. The SFE is estimated by the ratio of the luminosity produced by IR-selected, massive young stellar objects (MYSOs) and H II regions to the CO-traced mass in molecular clouds. In Sections 2 and 3 we describe the data and present the results. In Section 4 we discuss the findings and the implications for understanding the effect of Galactic structure on star formation.

2 DATA

The data used for this study consist of the sample of molecular clouds extracted from the ^{13}CO $J = 1 - 0$ Boston University/Five College Radio Astronomy Observatory Galactic Ring Survey (GRS; Jackson et al. 2006) by Rathborne et al. (2009) which have been positionally matched to mid-IR-selected, MYSOs and H II regions from the Red MSX Source (RMS) survey by (Urquhart et al. 2008; 2011). The result is a sample of molecular clouds with IR-detected high-mass star formation, as well as a complementary sample of clouds without RMS detections, all with kinematic distances, estimated cloud masses and total source luminosities. Distance ambiguities were resolved mainly by Roman-Duval et al. (2009) with additional determinations by Urquhart et al. (2011), in which details of the construction of the matched sample can also be found. The GRS cloud-mass estimates were revised upwards by a factor of several in a re-analysis by Roman-Duval et al. (2010). The spatial coverage of the data is $17°9 < l < 55°7$ and $|b| \leq 1°$, and the velocity range is -5 to $135\,\mathrm{km\,s^{-1}}$ for $l < 40°$ and -5 to $85\,\mathrm{km\,s^{-1}}$ at $l > 40°$, both set by the coverage of the GRS. The RMS sample is complete to $L_{\mathrm{bol}} > 10^4\,\mathrm{L_\odot}$ out to a heliocentric distance of $\sim 14\,\mathrm{kpc}$ and covers a Galactocentric radius (R_{GC}) range of 2.5–8.5 kpc. The combined sample consists of 176 RMS sources with 123 GRS cloud associations and 423 GRS clouds with no matching RMS detection above $10^4\,\mathrm{L_\odot}$.

Only GRS clouds with masses above $5 \times 10^4\,\mathrm{M_\odot}$ are included in the sample. This is a more conservative limit than adopted by Roman-Duval et al. (2010) ($1.1 \times 10^4\,\mathrm{M_\odot}$). The sample was also limited to sources with heliocentric distances greater than 2 kpc,

in order to remove local sources that might affect the results at $R_{\mathrm{GC}} \simeq 8\,\mathrm{kpc}$.

Source luminosities were obtained by constructing spectral energy distributions from various public data sources and fitting them with the YSO model fitter of Robitaille et al. (2006). Luminosities are effectively bolometric although necessarily dominated by IR data (see Mottram et al. 2011b for details).

3 ANALYSIS AND RESULTS

Fig. 1 shows the mean mass surface density of molecular gas in ^{13}CO-traced GRS clouds ($\Sigma_{M_{\mathrm{CO}}}$), selected as described in Section 2, as a function of R_{GC}. This result is the same as that in fig. 8 of Roman-Duval et al. (2010) and has been seen in a number of previous works (e.g. Liszt, Burton & Xiang 1984; Liszt 1993). There is a large peak in $\Sigma_{M_{\mathrm{CO}}}$ at $R_{\mathrm{GC}} = 4$–5 kpc. This region corresponds to the Scutum spiral-arm origin and inner tangent and the end of the Galactic bar at Galactic longitude $l \sim 30°$, where the massive star-forming regions W43 and G29.96 are located (see e.g. Bally et al., 2010; Nguyen-Luong et al. 2011). The Scutum arm material occupies a relatively large range of velocities and kinematic distances (Nguyen-Luong et al. 2011; Eden et al. 2012) but a much narrower range in R_{GC} and so is a well-defined feature using this scale.

At radii less than ~ 4 kpc, $\Sigma_{M_{\mathrm{CO}}}$ falls rapidly to comparatively very low values. At larger radii, $\Sigma_{M_{\mathrm{CO}}}$ declines slightly less steeply, with two additional peaks at $R_{\mathrm{GC}} = 6$–6.5 kpc and 7.5–8 kpc. These two zones correspond to the average radii of the inner segments of the Sagittarius and Perseus spiral arms, respectively, as they pass through the GRS region.

Fig. 2 shows the integrated luminosity of RMS MYSOs and H II regions per unit Galactic surface area ($\Sigma_{L_{\mathrm{bol}}}$) as a function of R_{GC}. Three peaks can again be identified in the distribution at 4–4.5, 6–6.5 and 7.5–8 kpc, corresponding to those seen in the $\Sigma_{M_{\mathrm{CO}}}$ distribution of Fig. 1. This time, however, the contrast between the three features is less marked and the contrast with the background levels is greater. The background level of $\Sigma_{L_{\mathrm{bol}}}$ also falls steadily with radius beyond $R_{\mathrm{GC}} \simeq 5$ kpc, but less steeply than the mass surface density. These features were also seen, in the same data by Urquhart et al. (2011).
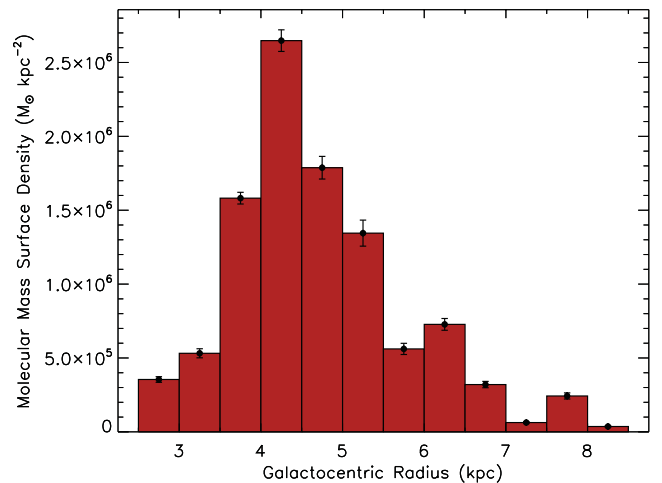

Figure 1. Galactic surface density of molecular mass in the GRS region as traced by clouds in the catalogue of Rathborne et al. (2009), using the revised masses of Roman-Duval et al. (2010) and a lower limit of $5 \times 10^4\,\mathrm{M_\odot}$ per cloud. The x-scale is Galactocentric radius and the bin size is 0.5 kpc. Errors are derived from the mass uncertainties listed by Roman-Duval et al. (2010).
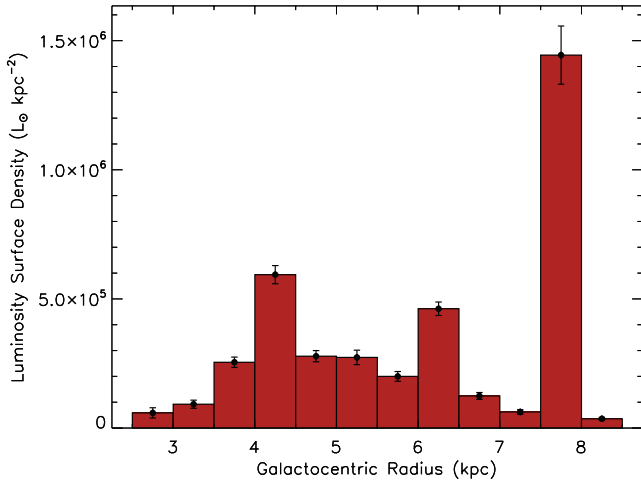
Figure 2. The Galactic surface density of RMS source luminosity above the completeness limit of $10^4\,L_\odot$, as a function of Galactocentric radius. Sources within 2 kpc of the Sun and those associated with GRS clouds of $M < 5 \times 10^4\,M_\odot$ have been removed. The error bars are based on the average uncertainty on the total IR luminosity of 34 per cent estimated by Mottram et al. (2011a).
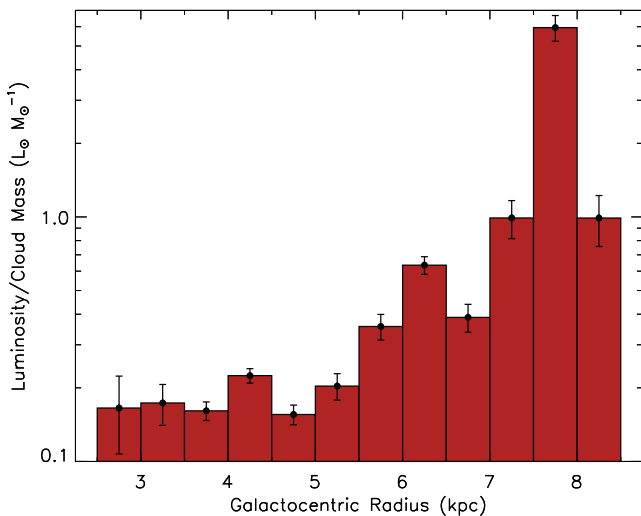

Figure 3. The ratio of integrated RMS source luminosity to mass in GRS clouds (L_{bol}/M_{CO}) as a function of Galactocentric radius. The y-scale is plotted logarithmically in order to show detail at low levels.

Fig. 3 presents the ratio of the total luminosity L_{bol} associated with RMS sources to total molecular mass M_{CO} in GRS clouds in each radial bin. From $R_{GC} = 2.5$ to 5.5 kpc, L_{bol}/M_{CO} has a low value ($\sim0.18\,L_\odot/M_\odot$) and is nearly flat and featureless. At $R_{GC} > 5.5$ kpc, L_{bol}/M_{CO} begins to rise and goes through two discrete, significant peaks, the first at $R_{GC} = 6$–6.5 kpc, where the value rises to $\sim0.63\,L_\odot/M_\odot$, 70 per cent higher than the adjacent bins, and a much stronger one of $\sim5.9\,L_\odot/M_\odot$ at $R_{GC} = 7.5$–8 kpc, around six times larger than in the bins either side. The latter two features again correspond to the radii of the Sgr and Per arms, respectively (see Fig. 4).

The GRS survey does not cover the two spiral arms beyond Perseus which are the Norma arm and the distant, outer Scutum–Centaurus arm recently detected by Dame & Thaddeus (2011). Although at least partly within its spatial range, these are both outside the solar circle and so at negative relative velocities, and
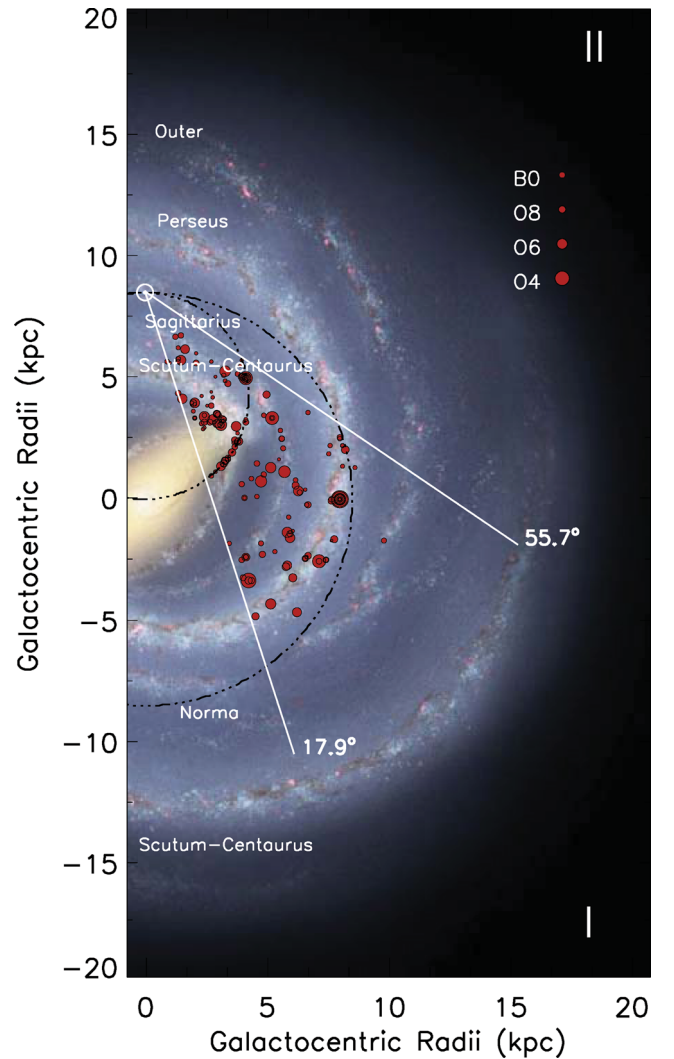

Figure 4. The distribution of RMS YSOs that have assigned distances within the GRS region, superimposed on part of the sketch plan of the Galaxy by Robert Hurt of the *Spitzer* Science Center, in consultation with Robert Benjamin. The key demonstrates the approximate luminosity of each RMS source. The figure is adapted from Urquhart et al. (2011).

thus not detected by the GRS. The outer Scutum–Centaurus arm also lies partly above the latitude range of the GRS, following the upward warp of the plane.

4 DISCUSSION

4.1 Star formation efficiency versus the MYSO luminosity function

The quantities plotted in Figs 1 and 2, $\Sigma_{M_{CO}}$ and $\Sigma_{L_{bol}}$, depend on the number density of molecular clouds as well as on any physical differences in the sources. Their ratio, L_{bol}/M_{CO} (Fig. 3), is independent of source crowding and therefore reveals differences in at least the outcome of the star formation process as a function of Galactic radius. L_{bol}/M_{CO} is determined by a combination of the mean SFE, which is the SFR per unit gas mass, integrated over the relevant time-scale, and the luminosity function (LF) of the massive young stars. If the SFE is high enough to cause significant

depletion of the molecular gas mass reservoir in a star formation time, its dependence on the SFR may become non-linear.

An increase in the value of L_{bol}/M_{CO} can therefore be produced by one or more of the following: a rise in the SFR per unit gas mass, a shallower LF (i.e. weighted towards high-luminosity sources) or a long time period. The time-scale sampled by the data is limited to the lifetimes of those evolutionary stages traced by the RMS survey. These are the MYSO and compact H II-region stages, the durations of which have both been determined to be $<5 \times 10^5$ yr by Mottram et al. (2011a). This time-scale is short enough, compared to the lifetime of a molecular cloud, that the data provide a snapshot of the current star formation. We therefore consider that it is not necessary to account for differing lengths of time over which star formation might have continued.

Where the LF of forming stars is invariant, the ratio L_{bol}/M_{CO} is simply a measure of the current SFE. In this case, Fig. 3 indicates a significantly higher SFE in the two outer spiral arms (Sgr and Per) compared to that in the region with $R_{GC} < 6$ kpc and, importantly, relative to that in the neighbouring inter-arm clouds. This suggests that physical conditions in the molecular clouds within these arms are altered in some way. Additionally, Fig. 3 shows that the average SFE is significantly higher in the inner Perseus arm compared to the inner Sgr arm, and so that conditions for star formation may be different from arm to arm.

Despite very strong peaks in both $\Sigma_{M_{CO}}$ and $\Sigma_{L_{bol}}$ at $R_{GC} = 4$–5 kpc (Figs 1 and 2), L_{bol}/M_{CO} in this inner region is low and nearly constant. These inner radii contain the Scutum spiral-arm tangent and the near end of the Galactic bar, including the massive star-forming regions W43 and G29.96. The former has been described as starburst like (e.g. Bally et al. 2010; Nguyen-Luong et al. 2011), but Fig. 3 implies that the intense concentration of star formation found there is largely the result of the huge amount of molecular gas along that line of sight and not to a significantly elevated SFE. This result is consistent with those of Eden et al. (2012), who find no significant difference between the mass fraction of dense clumps in the molecular clouds associated with W43 and that in the foreground and background clouds on the same line of sight.

While there is little strong observational evidence to support the hypothesis that the initial mass function (IMF) of massive stars is sensitive to the initial conditions for star formation (Bastian, Covey & Meyer 2010), it is still possible that L_{bol}/M_{CO} may also depend on the LF of the massive young stars that are forming. In such a case, the same SFE but with a flatter IMF would yield a higher value of L_{bol}/M_{CO}. Since the latter is made up of the number of YSOs formed per unit cloud mass and the LF of those YSOs, we can partly separate the two effects by examining independently the numbers of RMS sources per unit cloud mass, N_{RMS}/M_{CO}, and the RMS source LF.

Fig. 5 shows N_{RMS}/M_{CO} as a function of R_{GC}. Against a rising background value beyond $R_{GC} \simeq 5$ kpc, there is a small peak in N_{RMS}/M_{CO} at 6.0–6.5 kpc, the radius of the Sgr arm. The apparent significance of this peak is barely 3σ because of the large Poisson error bars, but it represents an increase of around 70 per cent over the neighbouring points and is enough to account for the peak in L_{bol}/M_{CO} at the same radius in Fig. 3. There is therefore no need to suspect any change in LF associated with the Sgr arm and an increase in the number of YSOs produced per unit gas mass, i.e. a simple increase in the SFE, appears to be a sufficient explanation. In contrast, Fig. 5 shows no evidence of any rise in N_{RMS}/M_{CO} in the $R_{GC} = 7.5$–8.0 kpc bin, and so a simple increase in SFE does not explain the large peak in L_{bol}/M_{CO} in the Per arm seen in Fig. 3 and we need to look for changes in the LF as a function of R_{GC}.
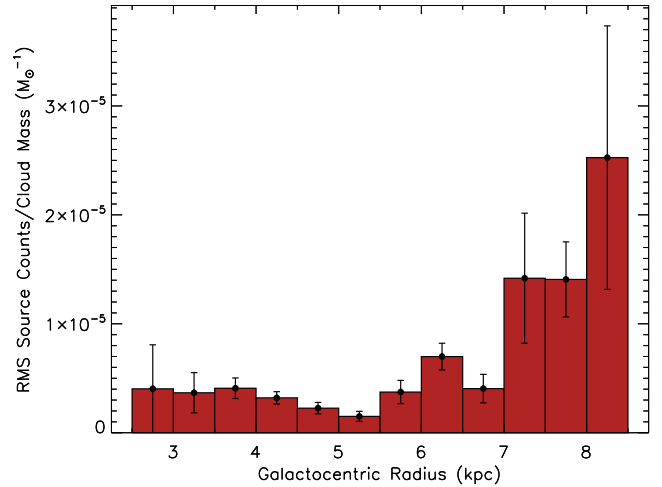

Figure 5. The number of RMS MYSO sources above 10^4 L$_\odot$ per unit molecular gas mass traced by GRS clouds (N_{RMS}/M_{CO}). The error bars represent Poisson errors on the RMS source counts combined with uncertainties on mass estimates from Roman-Duval et al. (2010), with the latter adjusted for a distance uncertainty of 1 kpc.

The LF of MYSOs has been determined for the whole Galaxy by Mottram et al. (2011a), but the present sample is not large enough to generate an explicit LF for each 0.5 kpc R_{GC} bin. However, we can crudely examine the LF as a function of R_{GC} via the mean luminosity $\langle L_{bol} \rangle$, both explicitly and by statistical tests for differences in the luminosity distributions.

Fig. 6 shows the value of $\langle L_{bol} \rangle$, i.e. the total L_{bol} divided by the number of RMS sources in each R_{GC} bin. This time we see a significant increase by a factor of ~ 7 at the 8-kpc radius of the Per arm but no change at the Sgr arm (6.5 kpc) and a flat or slowly rising value [$\sim(4-7) \times 10^4$ L$_\odot$] between 3 and 5 kpc. Some caution is required here, since the distribution of luminosities $N(L_{bol})$ is a power law with a lower cut-off imposed by incompleteness and an upper cut-off at $N = 1$, due to integer values of N. Hence L_{bol}/N is an increasing function of N, i.e. the sample size. If the power-law exponent is -1.5, then $\langle L_{bol} \rangle \propto N^{1/3}$ exactly. The normalized
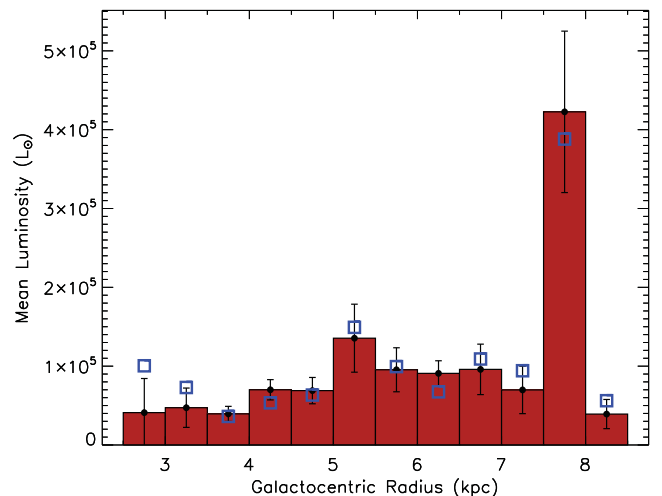

Figure 6. The mean luminosity of RMS sources ($\langle L_{bol} \rangle$) with $L_{bol} \geq 10^4$ L$_\odot$, as a function of Galactic radius, i.e. the total luminosity divided by the number of sources per bin. The blue squares show the effect of correcting for a $N^{1/3}$ dependence in $\langle L_{bol} \rangle$ (see text).
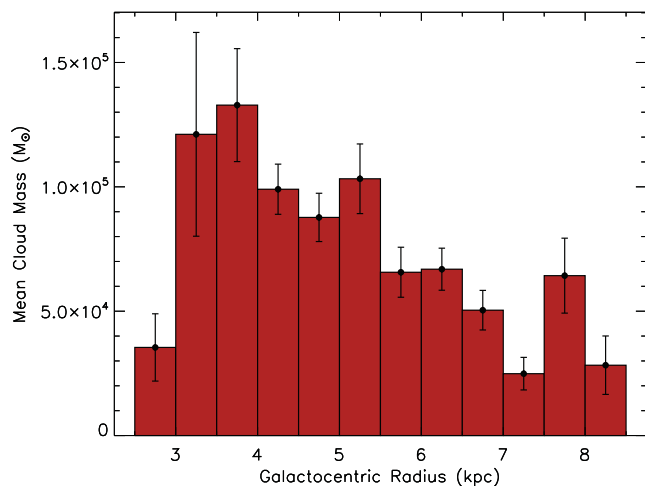
Figure 7. The average GRS cloud mass as a function of Galactocentric distance.

correction for this bias is shown in Fig. 6 but is obviously smaller than the $\sqrt{N}$ uncertainties on N. The true LF of RMS-traced massive star-forming regions may be shallower than this (Mottram et al. 2011a) and the severity of the bias rises sharply for exponents more positive than -1. However, since there are fewer RMS sources in the 7.5–8.0 kpc Perseus-arm bin (19) than in the Sagittarius- and Scutum-arm bins (36 and 33, respectively), such a bias cannot explain the much higher $\langle L_{bol}\rangle$ in the former. This result therefore implies a significant flattening of the MYSO LF in the Per arm.

Two statistical tests of the distribution of L_{bol} were performed, looking for differences between the RMS sources in the Perseus-arm subsample ($R_{GC} = 7.5-8.0$ kpc) and the rest of the sample. The Mann–Whitney U test, which is mainly sensitive to displacements (i.e. differences in the means) between two samples which are not normally distributed, produced a probability that the two samples come from the same distribution of $p = 0.0004$. The Kolmogorov–Smirnov test for general differences in the two distributions resulted in $p = 0.028$. The null hypothesis (that the samples come from the same distribution) can therefore be rejected at least at the 2σ level.

As well as the discrete features associated with the spiral arms, Figs 3 and 5 show a gradual increase in the baseline value of both L_{bol}/M_{CO} and N_{RMS}/M_{CO} by factors of about 5 between $R_{GC} = 4$ and 8 kpc. This gradient can be largely explained by Fig. 7, which shows a steady decrease, beyond $R_{GC} = 4$ kpc, in the mean molecular-cloud mass $\langle M_{CO}\rangle$ by a similar factor. The latter result was also seen by Roman-Duval et al. (2010) and will be discussed in more detail in a forthcoming paper. Fig. 7 also shows a discrete peak in $\langle M_{CO}\rangle$ at the radius of the Per arm, but none at the Sgr arm or the Scutum tangent region.

4.2 The effect of individual sources within the arms

The peaks in L_{bol}/M_{CO} at $R_{GC} \sim 6$ and 8 kpc are both due to the presence of individual star-forming complexes with very high local values of L_{bol}/M_{CO} within the corresponding spiral arms. At $\sim$6 kpc, W51A and W51B are associated with the GRS cloud G049.49–00.41 which has a Galactocentric distance of 6.5 kpc (Rathborne et al. 2009). The mass of this cloud is determined to be $(1.8 \pm 0.5) \times 10^5$ M$_\odot$ (Roman-Duval et al. 2010) and its integrated luminosity in RMS sources with $L > 10^4$ L$_\odot$ is estimated to be 1.37×10^6 L$_\odot$, giving $L_{bol}/M_{CO} = 7.6 \pm 2.3$ L$_\odot$ M$_\odot^{-1}$. Nine RMS sources are associated with this cloud (Urquhart et al. 2011), seven of which

are above the 10^4 L$_\odot$ completeness limit. Just three of these sources have luminosities above 10^5 L$_\odot$ (RMS 49.4903–00.3694, 49.5373–00.3929 and 49.4564–00.3559).

Kang et al. (2010) estimate the total molecular gas mass in W51 as 2.3×10^5 M$_\odot$ in at least eight clouds, while Carpenter & Sanders (1998) obtain 1.2×10^6 M$_\odot$. Harvey et al. (1986) set the total luminosity at 3×10^6 L$_\odot$, using an assumed distance of 7 kpc. The distance has been estimated by trigonometric parallax at 5.4 ± 0.3 kpc (Sato et al. 2010), which implies $R_{GC} = 6.3$ kpc. At this distance, the Harvey et al. luminosity estimate becomes 1.8×10^6 L$_\odot$. The molecular gas content of W51 has been studied in detail by Parsons et al. (2012).

At $R_{GC} \simeq 8$ kpc, the well-known star-forming region W49A is associated with GRS cloud G43.19–00.01, whose mass is $(2.2 \pm 0.3) \times 10^5$ M$_\odot$ and total RMS source luminosity is 6.87×10^6 L$_\odot$. This gives $L_{bol}/M_{CO} = 32 \pm 6$ L$_\odot$ M$_\odot^{-1}$. Nine RMS MYSOs are associated with this cloud, all with luminosity above 10^4 L$_\odot$. Five of these have $L > 10^5$ L$_\odot$ and the integrated luminosity is dominated by two sources (RMS 43.1679–00.0095 and 43.1650–00.0285) with $L_{bol} > 10^6$ L$_\odot$.

Roberts et al. (2011) suggest that W49A is a good Galactic analogue for an extragalactic starburst system, having gas temperatures of 50–100 K and densities $\sim$$10^6$ cm^{-3}. Its distance was determined from maser proper motions to be 11.4 ± 1.2 kpc (Gwinn, Moran & Reid 1992). Its total luminosity was estimated at 6×10^6 L$_\odot$ by Harvey, Campbell & Hoffman (1977) and at $>10^7$ L$_\odot$ by Sievers et al. (1991) and Ward-Thompson & Robson (1990) and it contains more than a dozen compact H II regions. It has been suggested that the high SFR in W49 is the result of a cloud–cloud collision resulting from orbit crowding in the spiral arm (Serabyn, Güsten & Schulz 1993). The total associated gas mass in several clouds in the region has been variously assayed at 1.7×10^6 M$_\odot$ (Miyawaki, Hayashi & Hasegawa 2009) and 1.1×10^6 M$_\odot$ (Williams, Dickel & Auer 2004).

If we remove the GRS cloud containing the W49A RMS sources, the $R_{GC} = 7.5-8.0$ kpc bin then has integrated $L_{bol}/M_{CO} = 1.03 \pm 0.15$ L$_\odot$ M$_\odot^{-1}$, $N_{RMS}/M_{CO} = (0.9 \pm 0.3) \times 10^{-5}$ M$_\odot^{-1}$ and $\langle L_{bol}\rangle = (1.1 \pm 0.4) \times 10^5$ L$_\odot$, similar to the levels in the adjacent bins in each case (Figs 3, 5 and 6). Removing the cloud associated with W51A and B, the 6.0–6.5 kpc bin has $L_{bol}/M_{CO} = 0.38 \pm 0.03$ L$_\odot$ M$_\odot^{-1}$, $N_{RMS}/M_{CO} = (0.5 \pm 0.1) \times 10^{-5}$ M$_\odot^{-1}$ and $\langle L_{bol}\rangle = (6.5 \pm 1.3) \times 10^4$ L$_\odot$, which results in a slightly reduced peak in L_{bol}/M_{CO}, relative to the neighbouring bins. This suggests that, without W51, the Sgr arm still has somewhat increased SFE, while the Per arm has a flatter than normal LF solely due to the presence of the W49A MYSOs.

4.3 Implications for the effect of spiral-arm structure on star formation

What does the foregoing analysis tell us about spiral arms as potential large-scale triggers of star formation? Fig. 2 shows increases in $\Sigma_{L_{bol}}$ by factors of about 2.2, 2.9 and 30 in the Scu, Sgr and Per arm segments, respectively, relative to the adjacent inter-arm regions. Around 70, 60 and 80 per cent, again respectively, of these rises are due to simple source crowding. The remaining 20–40 per cent of the increase in $\Sigma_{L_{bol}}$ is due to changes in the luminosity per unit cloud mass and may be associated with a physical effect on the clouds caused by the presence of the arms.

There is some indication in Fig. 7 that cloud masses may be larger in the Per spiral arm, while no similar increase is seen in the Sgr arm. This may be an indication that clouds within the Per arm, or

at least in W49, may be in an altered state. If clouds are more massive, they may be less well supported on large scales. Interestingly, the simulations of Krumholz, Klein & McKee (2011) predict that global collapse of massive molecular clouds with radiative feedback should produce a top-heavy stellar IMF because of the suppression of fragmentation of the cloud, while accretion on to the forming protostars continues. The overall SFE is not significantly affected.

Models by Dobbs et al. (2008) predict that smaller clouds aggregate into larger ones within spiral arms and, as they leave the arms, clouds are subject to shear and lose molecular gas. Dobbs et al. (2011) suggest that, while more massive GMCs accumulate in the arms, there is no direct effect on the SFR, only an indirect influence via longer lived and more strongly bound clouds. Pathological SF regions like W49A may be due to cloud–cloud collisions made more likely by longer cloud lifetimes and orbit crowding within spiral arms.

There is no clear evidence in the current results that can distinguish between changes in the clouds, caused by being within an arm, and increased triggered star formation caused by higher feedback between crowded star-forming regions. However, the lack of significant increases in L_{bol}/M_{CO} in the crowded Scutum tangent region suggests that feedback between clouds is not the dominant factor. Dib et al. (2012) found no significant connection between the shear resulting from the Galactic rotation and the SFE in the GRS molecular clouds.

The Scutum tangent lies at the bar end where there should be corotation between the pattern speed of the bar and the ISM. We might expect an altered star-forming environment in this region, at least from either the permanent presence of the bar potential and/or collisions between clouds in the circular orbits just outside the bar and gas following the x_1 orbits within it, as they reach the bar end. On the other hand, since the CO mass surface density is seen to drop rapidly inside 3 kpc, there may not be enough molecular gas in the bar for this to be a significant effect.

5 CONCLUSIONS

Around 70 per cent of the increase in the SFR density in spiral arms is due to simple source crowding within the arms. The remaining $\sim$30 per cent is the result of an increase in the luminosity coming from embedded MYSOs, relative to the mass of molecular gas present. In the segment of the Sagittarius spiral arm included in the GRS data, this increase in L_{bol}/M_{CO} is accounted for by a rise in the number of MYSOs per unit molecular gas mass, with no detected change in their mean luminosity compared to the nearby inter-arm areas. This implies an increase in the basic SFE in molecular clouds in the Sgr arm, and this is probably caused by a higher SFR per unit gas mass, given the short time-scales sampled by the RMS data, without any change in LF. In the Perseus arm segment, no increase in the number of RMS sources per unit cloud mass is detected, relative to the nearby inter-arm regions. Instead, the rise in L_{bol}/M_{CO} is wholly accounted for by an increase in the average luminosity of the MYSOs which implies a significant change in the average LF, i.e. in the IMF. Further, the changes in the Per arm are attributed wholly to the W49A star-forming complex. If this were removed from the data, star formation in the Per arm would be similar to that in the inter-arm gas. W49A appears to contain unusual star formation and may be genuinely starburst like, while the major star-forming regions in Sgr (W51) and Scu (W43) may be part of a normal distribution of star formation properties.

Compared to Foyle et al. (2010), who measured increases in SFR/M of less than 10 per cent in the arms of external spiral galaxies,

compared to inter-arm regions, our results show larger increases of $\sim$30 per cent in the Sgr and Per arms. In the Scutum tangent region, however, the enhancement in SFR density is almost entirely due to source crowding. This indicates variations within and between arms and that it is important to consider the scale to which such results correspond.

REFERENCES

Bally J. et al., 2010, A&A, 518, 90
Bastian N., Covey K. R., Meyer M. R., 2010, ARA&A, 48, 339
Benjamin R. A. et al., 2005, ApJ, 630, L149
Carpenter J. M., Sanders D. B., 1998, AJ, 116, 1856
Dame T. M., Thaddeus P., 2011, ApJ, 734, L24
Dib S., Walcher C. J. Heyer M., Audit E., Loinard L., 2009, MNRAS, 398, 1201
Dib S., Helou G., Moore T. J. T., Urquhart J. S., Dariush A., 2012, ApJ, (arXiv:1202.4699)
Dobbs C. L., Bonnell I. A., Pringle J. E., 2006, MNRAS, 371, 1663
Dobbs C. L., Glover S. C. O., Clark P. C., Klessen R. S., 2008, MNRAS, 389, 1097
Dobbs C. L., Burkert A., Pringle J. E., 2011, MNRAS, 417, 1318
Eden D. J., Moore T. J. T., Plume R., Morgan L. K., 2012, MNRAS, 422, 3178
Foyle K., Rix H.-W., Walter F., Leroy A. K., 2010, ApJ, 725, 534
Gwinn C. R., Moran J. M., Reid M. J., 1992, ApJ, 393, 149
Harvey P. M., Campbell M. F., Hoffmann W. F., 1977, ApJ, 215, 151
Harvey P. M., Joy M., Lester D. F., Wilking B. A., 1986, ApJ, 300, 737
Heyer M. H., Terebey S., 1998, ApJ, 502, 265
Jackson J. M. et al., 2006, ApJS, 163, 145
Kang M., Bieging J. H., Kulesa C. A., Lee Y., Choi M., Peters W. L., 2010, ApJS, 190, 58
Kobayashi N., Yasui C., Tokunaga A. T., Saito M., 2008, ApJ, 683, 178
Krumholz M. R., McKee C. F., Tumlinson J., 2009, ApJ, 669, 850
Krumholz M. R., Cunningham A. J., Klein R. I., McKee C. F., 2010, ApJ, 713, 1120
Krumholz M. R., Klein R. I., McKee C. F., 2011, ApJ, 740, 74
Lépine J. R. D. et al., 2011, MNRAS, 417, 698
Leroy A. K., Walter F., Brinks E., Bigiel F., de Blok W. J. G., Madore B., Thornley M. D., 2008, AJ, 136, 2782
Liszt H., 1993, ApJ, 411, 720
Liszt H., Burton W. B., Xiang D.-L., 1984, A&A, 140, 303
Miyawaki R., Hayashi M., Hasegawa T., 2009, PASJ, 61, 39
Mottram J. C. et al., 2011a, ApJ, 730, 33
Mottram J. C. et al., 2011b, MNRAS, 525, 149
Nguyen-Luong Q. et al., 2011, A&A, 529, 41
Parsons H., Thompson M. A., Clark J. S., Chrysostomou A. C., 2012, MNRAS, 424, 1658
Rathborne J. M., Johnson A. M., Jackson J. M., Shah R. Y., Simon R., 2009, ApJS, 182, 131

Roberts H., van der Tak F. F. S., Fuller G. A., Plume R., Bayet E., 2011, A&A, 525, 107

Robitaille T. P., Whitney B. A., Indebetouw R., Wood K., Denzmore P., 2006, ApJS, 167, 256

Roman-Duval J., Jackson J. M., Heyer M., Johnson A., Rathborne J., Shah R., Simon R., 2009, ApJ, 699, 1153

Roman-Duval J., Jackson J. M., Heyer M., Rathborne J., Simon R., 2010, ApJ, 723, 492

Sato M., Reid M. J., Brunthaler A., Menten K. M., 2010, ApJ, 720, 1055

Serabyn E., Güsten R., Schulz A., 1993, ApJ, 413, 571

Sievers A. W., Mezger P. G., Bordeon M. A., Kreysa E., Haslam C. G. T., Lemke R., 1991, A&A, 251, 231

Urquhart J. S., Hoare M. G., Lumsden S. L., Oudmaijer R. D., Moore T. J. T., in Beuther H., Linz H., Henning T., eds, ASP Conf. Ser. Vol. 387, Massive Star Formation: Observations Confront Theory. Astron. Soc. Pac., San Francisco, p. 381

Urquhart J. S. et al., 2011, MNRAS, 410, 1237

Ward-Thompson D., Robson E. I., 1990, MNRAS, 244, 458

Williams J. A., Dickel H. R., Auer L. H., 2004, ApJS, 153, 463

This paper has been typeset from a TEX/LATEX file prepared by the author.